

# Radioactive decay products in neutron star merger ejecta: heating efficiency and $\gamma$ -ray emission

K. Hotokezaka<sup>\*1</sup>, S. Wanajo<sup>2,3</sup>, M. Tanaka<sup>4</sup>, A. Bamba<sup>5</sup>, Y. Terada<sup>6</sup>, and T. Piran<sup>1</sup>

<sup>1</sup>*Racah Institute of Physics, The Hebrew University of Jerusalem, Jerusalem 91904, Israel.*

<sup>2</sup>*Department of Engineering and Applied Sciences, Sophia University, Chiyoda-ku, Tokyo 102-8554, Japan.*

<sup>3</sup>*iTHES Research Group, RIKEN, Wako, Saitama 351-0198, Japan.*

<sup>4</sup>*National Astronomical Observatory of Japan, Mitaka, Tokyo 181-8588, Japan.*

<sup>5</sup>*Department of Physics and Mathematics, Aoyama Gakuin University 5-10-1 Fuchinobe Chuo-ku, Sagami-hara, Kanagawa 252-5258, Japan.*

<sup>6</sup>*Graduate School of Science and Engineering, Saitama University, 255 Shimo-Okubo, Sakawa, Saitama, Saitama 338-8570, Japan.*

17 Nov, 2015

## ABSTRACT

The radioactive decay of the freshly synthesized  $r$ -process nuclei ejected in compact binary mergers power optical/infrared macronovae (kilonovae) that follow these events. The light curves depend critically on the energy partition among the different products of the radioactive decay and this plays an important role in estimates of the amount of ejected  $r$ -process elements from a given observed signal. We study the energy partition and  $\gamma$ -ray emission of the radioactive decay. We show that 20–50% of the total radioactive energy is released in  $\gamma$ -rays on timescales from hours to a month. The number of emitted  $\gamma$ -rays per unit energy interval has roughly a flat spectrum between a few dozen keV and 1 MeV so that most of this energy is carried by  $\sim 1$  MeV  $\gamma$ -rays. However at the peak of macronova emission the optical depth of the  $\gamma$ -rays is  $\sim 0.02$  and most of the  $\gamma$ -rays escape. The loss of these  $\gamma$ -rays reduces the heat deposition into the ejecta and hence reduces the expected macronova signals if those are lanthanides dominated. This implies that the ejected mass is larger by a factor of 2–3 than what was previously estimated. Spontaneous fission heats up the ejecta and the heating rate can increase if a sufficient amount of transuranic nuclei are synthesized. Direct measurements of these escaping  $\gamma$ -rays may provide the ultimate proof for the macronova mechanisms and an identification of the  $r$ -process nucleosynthesis sites. However, the chances to detect these signals are slim with current X-ray and  $\gamma$ -ray missions. New detectors, more sensitive by at least a factor of ten, are needed for a realistic detection rate.

**Key words:** gravitational waves—binaries:close—stars:neutron—gamma-ray burst:general

## 1 INTRODUCTION

The origin of a half of the elements heavier than iron such as gold and uranium, which are made by the  $r$ (apid)-process, is one of the current nucleosynthesis long-standing mysteries (Cowan et al. 1991; Wanajo & Ishimaru 2006; Qian & Wasserburg 2007; Arnould et al. 2007). Compact binary mergers (neutron star–neutron star or neutron star–black hole binaries) that eject highly neutron rich material in which  $r$ -process nucleosynthesis would naturally take place have been suggested as promising production sites (Lattimer & Schramm 1976; Symbalisty & Schramm 1982; Eichler et al. 1989; Freiburghaus et al. 1999).

While the overall amount of heavy  $r$ -process material in the Galaxy is consistent with expectations of mass ejection in mergers and with their expected rates (see, e.g., Kalogera et al. 2004; Kim et al. 2015; Wanderman & Piran 2015 for the merger rate estimates), Argast et al. (2004) pointed out a difficulty for neutron star mergers to reproduce the  $r$ -element enrichment for halo stars with very low metallicities due to the delay time of the merger events. This difficulty can be resolved by taking into account the turbulent mixing of material in the galaxy (Piran et al. 2014), the assembly of sub-halos during the formation of the Galaxy (van de Voort et al. 2015; Ishimaru et al. 2015; Shen et al. 2015; Hirai et al. 2015) or if the delay time of mergers in the early Universe is shorter than what current models suggest. The large scatter in the abun-

\* E-mail: kenta.hotokezaka@mail.huji.ac.il

dances of  $r$ -process elements of metal poor stars can be naturally explained by the rarity of  $r$ -processing events such as neutron star mergers (e.g., Tsujimoto & Shigeyama 2014; Wehmeyer et al. 2015). In addition, Hotokezaka et al. (2015) have shown that the rarity of the merger events is broadly consistent with the  $^{244}\text{Pu}$  abundances of the early solar system material (Turner et al. 2007) and the present-day deep-sea archives (Wallner et al. 2015).

The merger origin scenario of  $r$ -process elements has been attracting even more attention since the discovery of a possible macronova, also called as a kilonova, associated with the short gamma-ray burst (GRB) 130603B (Tanvir et al. 2013; Berger et al. 2013). More recently, it has been shown that there is an infrared excess in the afterglow data of GRB 060614 (Yang et al. 2015) as well, suggesting another macronova candidate. A macronova is a radioactively powered transient as an electromagnetic signal of  $r$ -process elements in merger ejecta (Li & Paczyński 1998; Metzger et al. 2010; Roberts et al. 2011; Korobkin et al. 2012; Barnes & Kasen 2013; Tanaka & Hotokezaka 2013; Grossman et al. 2014; Kasen et al. 2015). While both candidates are based on single data points, the observed data are largely consistent with theoretical expectations of macronovae and, if correct, it is a strong evidence that compact binary mergers eject significant amounts of  $r$ -process material. The association of these macronovae with short GRBs provide the first direct evidence, supporting the circumstantial evidence (Nakar 2007; Berger 2014), that compact binary mergers are the progenitors of short gamma-ray bursts (Eichler et al. 1989).

The minimal required mass to explain the brightness of the macronova candidate associated with GRB 130603B is estimated as  $0.02 M_{\odot}$  (Hotokezaka et al. 2013a; Piran et al. 2014). This is consistent with recent hydrodynamical simulations of compact binary mergers (Hotokezaka et al. 2013; Bauswein et al. 2013; Rosswog 2013; Foucart et al. 2013; Fernández & Metzger 2013; Metzger & Fernández 2014; Perego et al. 2014; Just et al. 2015; Kyutoku et al. 2015; Sekiguchi et al. 2015; Kawaguchi et al. 2015; Kiuchi et al. 2015; East et al. 2015). The minimal required mass for the macronova candidate associated with GRB 060614 is even larger of order  $0.1 M_{\odot}$  (Yang et al. 2015) and this can possibly be explained only in a neutron star-black hole merger (Foucart et al. 2013; Just et al. 2015; Kyutoku et al. 2015; Kiuchi et al. 2015).

Estimates of the mass of ejected  $r$ -process elements depend not only on the overall energy generation rate of the radioactive decay but also on the efficiency that the energy of emitted decay products is deposited in the ejecta. While the overall energy generation rate has been extensively studied (Metzger et al. 2010; Roberts et al. 2011; Korobkin et al. 2012; Wanajo et al. 2014; Lippuner & Roberts 2015), the heating efficiency has not been well studied. In the literature, it is often assumed that 30–50% of the generated energy is deposited in the ejecta. In order to evaluate the efficiency, one needs to identify the energies released in different decay products: electrons, neutrinos,  $\gamma$ -rays, fission fragments, and  $\alpha$ -particles. Here we determine the energy partition among the different types of products and estimate the net energy deposition rate in the ejecta. We pay particular attention to the escape

of  $\gamma$ -rays from the ejecta at the stage when it is still optically thick to IR/optical/UV radiation.

In addition, it is worthwhile to study the spectrum and flux of the  $\gamma$ -rays escaping from the macronova. The detection of  $\gamma$ -ray lines of specific heavy nuclei can provide a conclusive evidence for  $r$ -processing during a merger event. While the detection of  $\gamma$ -ray lines of radioactive decay from astrophysical sources is quite challenging, they have been detected from nearby supernovae: the  $\gamma$ -ray lines of  $^{56}\text{Co}$  from the type II SN 1987A (Matz et al. 1988; Teegarden et al. 1989) and those of  $^{56}\text{Ni}$  and  $^{56}\text{Co}$  from the type Ia SN 2014J (Diehl et al. 2014; Churazov et al. 2014; Terada et al. 2015). Due to the rarity of macronova this detection is even more challenging. Still it is interesting to discuss the expected observational features of  $\gamma$ -ray lines of  $r$ -process nuclides from neutron star mergers and their detectability with current and future X-ray and  $\gamma$ -ray facilities.

## 2 MODEL SET UP

The abundance pattern of synthesized nuclei in merger ejecta depends on the fluid element’s initial state, expansion velocity, and neutrino irradiation from the central remnant object (Freiburghaus et al. 1999; Metzger et al. 2010; Roberts et al. 2011; Korobkin et al. 2012; Wanajo et al. 2014; Goriely et al. 2015). Although the resulting patterns obtained from such merger models are not necessarily similar to the solar  $r$ -process abundance pattern, it is known that the abundances of  $r$ -process elements in  $r$ -process-enhanced stars in the Galactic halo closely follow the solar  $r$ -process one, in particular for  $Z > 50$  with almost perfect agreement (see, e.g., Sneden et al. 2008; Barbuy et al. 2011; Roederer et al. 2014; Siqueira Mello et al. 2014). This fact suggests that a single phenomena reproduces the solar-like  $r$ -process abundance patterns.

We assume (see Tanaka et al. 2014), therefore, that the nuclear abundance distribution ( $Y_A$ , in the range  $90 \leq A \leq 238$  for the fiducial case, see below) that matches the solar pattern of stable and long-lived ( $^{232}\text{Th}$  and  $^{235,238}\text{U}$ )  $r$ -process nuclei (Cowan et al. 1999). Nuclear abundances ( $Y_A = \sum_Z Y_{Z,A}$ ) are thus time-independent while isotopic abundances ( $Y_{Z,A}$ ) are time-dependent. The initial  $Z$  for each  $Y_{Z,A}$  is set at the neutron separation energy of about 2 MeV (roughly at the  $r$ -process freezeout) in the very neutron-rich side of the chart of nuclides. The time evolution of all isotopes is then calculated by a reaction network code described in Wanajo et al. (2014). All the reaction channels except for  $\beta$ -decays (that do not change  $Y_A$ ) are switched off (for  $A < 206$ , see below). Uncertainties in theoretical estimates of  $\beta$ -decay lifetimes are irrelevant here because most of the isotopes decay back to the vicinity of  $\beta$ -stability after several seconds, where experimental half-lives and  $Q_{\beta}$ -values are available. Then we determine the energy partition into each type of decay product and the resulting  $\gamma$ -ray spectra. Here we use the nuclear data base Evaluated Nuclear Data File ENDF/B-VII.1 library<sup>1</sup> for electrons, neutrinos, and  $\gamma$ -rays.

<sup>1</sup> <https://www-nds.iaea.org/public/download-endf/ENDF-B-VII.1/decay/>

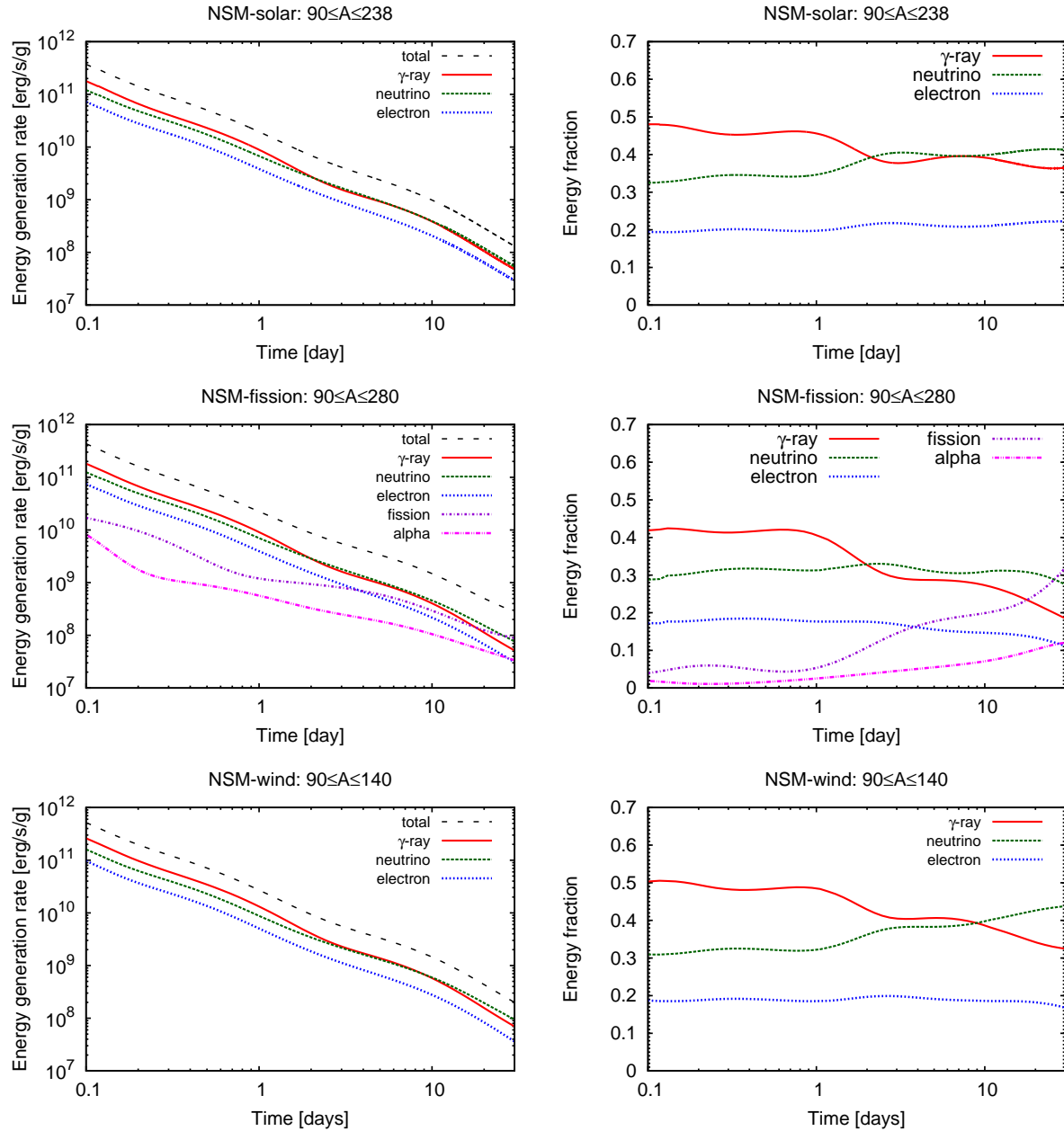


**Figure 1.** Energy generation rate in each type of particles (left) and its fraction to the total one (right) for NSM-solar ( $90 \leq A \leq 238$ ), NSM-fission ( $90 \leq A \leq 280$ ), and NSM-wind ( $90 \leq A \leq 140$ ) from the top to the bottom. Each curve shows the total rate (black long-dashed), those in the forms of  $\gamma$ -rays (red solid), neutrino (green dashed), electrons (blue dotted), fission fragments (violet dash-dotted), and  $\alpha$  particles (magenta dash-two dotted).

Although there are no stable (long-lived) nuclides with mass numbers above  $A = 238$  on Earth, some short-lived transuranic nuclei with  $A > 238$  are likely produced by the  $r$ -process. For example, there is clear evidence that  $^{244}\text{Pu}$  and  $^{247}\text{Cm}$  (with the half-lives of 81 Myr and 16 Myr, respectively) existed in the early solar system (Turner et al. 2004; Brennecka et al. 2010) and  $^{244}\text{Pu}$  is found in the Earth's material at present (Wallner et al. 2015). Furthermore, nucleosynthesis studies of merger ejecta show that very heavy nuclei up to mass numbers of  $\sim 280$  exist at the  $r$ -process freezeout (see, e.g., Goriely et al. 2013; Eichler et al. 2015). The spontaneous fission of such very heavy nuclei is also

suggested to affect the heating rate (Metzger et al. 2010; Wanajo et al. 2014). In this work, we study three cases:  $r$ -process nuclear distributions of (i) NSM (Neutron Star Merger)-solar:  $90 \leq A \leq 238$  (fiducial), (ii) NSM-fission:  $90 \leq A \leq 280$ , and (iii) NSM-wind:  $90 \leq A \leq 140$ . The last case, NSM-wind corresponds to the conditions within a possible lanthanide-free composition (from the wind, see below). For NSM-fission, we add the transuranic nuclei by assuming a constant  $Y_A$ 's of  $3.6 \cdot 10^{-4}$  for  $206 \leq A \leq 280$ . These values are taken so that the solar abundance of  $^{209}\text{Bi}$  is reproduced after nuclear decay. Note that the bulk of  $^{206,207,208}\text{Pb}$ ,  $^{209}\text{Bi}$ ,  $^{232}\text{Th}$ , and  $^{235,238}\text{U}$  are the ( $\alpha$  and  $\beta$ )

decayed products of actinides with  $209 < A < 254$ . The reaction network includes the channels for ( $\beta$ -delayed and spontaneous) fission and  $\alpha$ -decay in addition to  $\beta$ -decay for this mass region.

To study the heating efficiencies and resulting  $\gamma$ -ray line fluxes, one needs to specify the ejecta properties, e.g., the mass  $M_{\text{ej}}$  and expansion velocity  $v$ . In this work, we consider two types of merger ejecta: dynamical ejecta induced by tidal torque and shock heating during the merger (Hotokezaka et al. 2013; Bauswein et al. 2013; Rosswog 2013; Foucart et al. 2013; Kyutoku et al. 2015; Sekiguchi et al. 2015; Kawaguchi et al. 2015; East et al. 2015) and a wind ejected by neutrino heating, viscosity, magnetic field, and nuclear recombination from the remnant central object and its accretion disk (Shibata et al. 2011; Wanajo & Janka 2012; Fernández & Metzger 2013; Metzger & Fernández 2014; Perego et al. 2014; Siegel et al. 2014; Just et al. 2015; Kiuchi et al. 2015). We set as canonical parameters  $(M_{\text{ej}}, v) = (0.01M_{\odot}, 0.3c)$  for the dynamical ejecta and  $(0.01M_{\odot}, 0.05c)$  for the wind. We also consider an ejecta mass of  $0.1M_{\odot}$  as an extreme case. Such a large mass ejection may take place at a black-hole neutron star merger (Foucart et al. 2013; Just et al. 2015; Kyutoku et al. 2015; Kiuchi et al. 2015).

### 3 ENERGY PARTITION OF RADIOACTIVE DECAY INTO DIFFERENT TYPES OF PRODUCTS

Decay channels of freshly synthesized  $r$ -process nuclei are divided into the three types:  $\beta$ -decay,  $\alpha$ -decay, and spontaneous fission<sup>2</sup>. Different types of decay produce different types of products with different amounts of energy. A single  $\beta$ -decay emits one electron and one neutrino at energies of  $\sim 0.1$ –10 MeV. In addition to  $\beta$ -decay, heavy nuclei with  $A \geq 210$  are unstable to  $\alpha$ -decay or to spontaneous fission since the binding energy of such a nucleus appreciably decreases with the proton number due to the Coulomb repulsion. For both types of decay, the binding energy difference between the initial and final state of an emitted particle is about a few MeV per nucleon. Therefore a single decay releases about 5 MeV in kinetic energy for  $\alpha$ -decay and 200 MeV for spontaneous fission, respectively. Furthermore, all types of decay often leave excited nuclei that emit  $\gamma$ -rays as they transit to the ground states. The timescales of the transitions are much shorter than those in which we are interested in here. The energies of emitted  $\gamma$ -rays, which correspond to the differences between the energy levels of nuclides, range from a few dozen keV to a few MeV.

It is important to note that a single spontaneous fission process releases a huge amount of energy that is comparable to the energy released by  $\beta$ -decay of the sum of 10–100 nuclei. It is also worthy to note the time evolution of energy generation rate for each type of decay. For  $\alpha$ -decay and spontaneous fission, the energy generation rate evolves as  $\propto t^{-1}$  since each unstable nucleus releases roughly a fixed amount

of energy on the timescale of its lifetime. On the contrary,  $\beta$ -decay generates energy following roughly  $\propto t^{-1.3}$ . This is because for  $\beta$ -decay the nucleus with a longer lifetime releases a smaller amount of energy. Thus, depending on the abundance of transuranic elements, spontaneous fission potentially plays an important role in the macronova heating process at late times.

Figure 1 depicts the energy generation rates in different types of products resulting from  $r$ -process material (left). Roughly speaking, the energy generation rates in the forms of  $\gamma$ -rays (red solid curve), neutrinos (green dashed curve), and electrons (blue dotted curve) follow a power law of  $t^{-1.3}$ . For NSM-fission, the energy generation rates in spontaneous fission (violet dash-dotted curve) and  $\alpha$ -decay (magenta dash-two dotted curve) follows roughly  $\propto t^{-1}$  as anticipated. After around 5 days, the energy released in the form of fission fragments exceed the energy released in electrons. The right panels of Fig. 1 show the energy fractions released in all types of decay products. The energy fractions of neutrinos and  $\gamma$ -rays are 0.25–0.4 and 0.2–0.5, respectively. For NSM-solar and NSM-wind, the energy fraction of electrons is  $\sim 0.2$  and almost constant with time. For NSM-fission, the energy fraction of electrons slowly decreases with time from 0.2 to 0.1. After a few days, spontaneous fission releases 10–35% of the total radioactive energy. Note that the energy fraction of electrons is rather small compared to the typical value of  $\beta$ -decay. This small fraction is resulted from properties of nuclides around the second  $r$ -process peak  $A \sim 130$ . Some of them have larger  $Q_{\beta}$ -values and emit  $\gamma$ -rays at higher energies.

In Fig. 2, we show the  $\gamma$ -ray spectra for NSM-solar at 1 day, 3 days, 5 days, and 10 days after the merger. The black lines in each panel corresponds to the  $\gamma$ -ray spectrum at the fluid rest frame. The red (blue) curve is a spectrum taking into account the Doppler effect with an expansion velocity of  $v = 0.3c$  ( $0.05c$ ). Here each line is convolved with a Gaussian with a full-width-half-maximum of  $2\sqrt{\ln 2}v/c$ . The spectra are normalized with an ejecta mass of  $r$ -process elements of  $0.01M_{\odot}$  for an observer at a distance of 3 Mpc. The spectral shape is approximately flat from a few dozen keV to a few MeV and most of the  $\gamma$ -rays' energy is carried by photons at energies of  $\sim 1$  MeV. The spectrum is not significantly different among the different models as long as the second  $r$ -process peak ( $A \sim 130$ ) is contained as in our models.

On the timescales of interest for us, neutrinos completely escape from the ejecta without any interaction. Some of the  $\gamma$ -rays escape as well. Electrons,  $\alpha$ -particles, and fission fragments interact with charged particles via Coulomb collision and their energies may be deposited efficiently in the ejecta. The radioactive heating rate of the ejecta  $\dot{Q}$  can be written as

$$\dot{Q}(t) = \dot{E}_e(t) + \epsilon_{\gamma}(t)\dot{E}_{\gamma}(t) + \dot{E}_{\alpha}(t) + \dot{E}_f(t), \quad (1)$$

where  $\dot{E}_e$ ,  $\dot{E}_{\gamma}$ ,  $\dot{E}_{\alpha}$ , and  $\dot{E}_f$  are the energy generation rates in the forms of electrons,  $\gamma$ -rays,  $\alpha$ -particles, and fission fragments, respectively. We assume all the energy of charged decay products are deposited in the ejecta. For NSM-fission,

<sup>2</sup> Other channels such as neutron-induced fission,  $\beta$ -delayed fission, and  $\beta$ -delayed neutron emission play roles during or immediately after the  $r$ -process, which are irrelevant to macronova emission (some days after the merging).

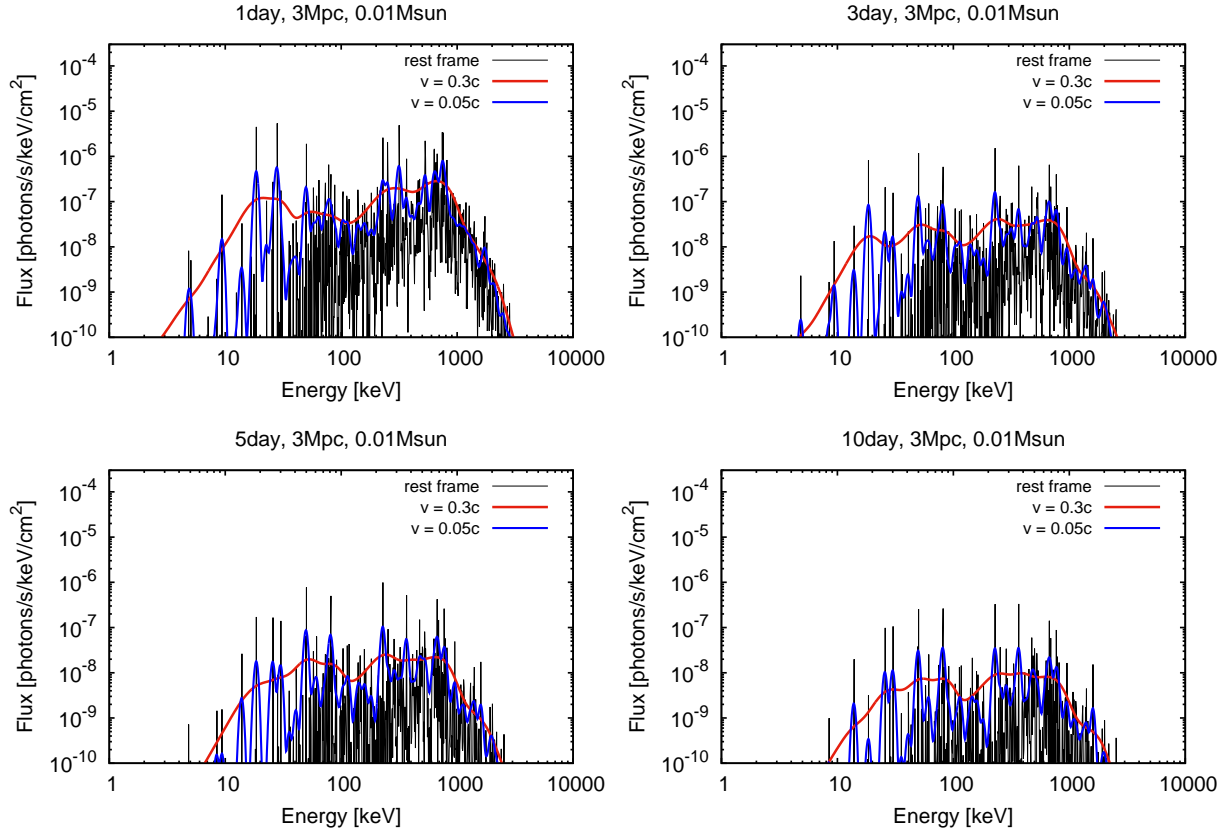


**Figure 2.** Spectrum of  $\gamma$ -rays at 1, 3, 5 and 10 days after merger for NSM-solar. Black lines depict the  $\gamma$ -ray spectrum produced by nuclei at rest. The red (blue) curve shows the spectrum with the Doppler broadening with an expansion velocity of 0.3c (0.05c). The normalization is determined with the mass of ejected  $r$ -process elements of  $0.01M_{\odot}$  and the observed distance of 3 Mpc. Here we do not take any absorption and scattering processes into account.

we find

$$\dot{E}_e(t) \approx 4 \cdot 10^9 \text{ erg/s/g} \left( \frac{t}{1 \text{ day}} \right)^{-1.3}, \quad (2)$$

$$\dot{E}_{\gamma}(t) \approx 8 \cdot 10^9 \text{ erg/s/g} \left( \frac{t}{1 \text{ day}} \right)^{-1.3}, \quad (3)$$

$$\dot{E}_{\alpha}(t) \approx 7 \cdot 10^8 \text{ erg/s/g} \left( \frac{t}{1 \text{ day}} \right)^{-1} \left( \frac{X_{A \geq 210}}{3 \cdot 10^{-2}} \right), \quad (4)$$

$$\dot{E}_f(t) \approx 2 \cdot 10^9 \text{ erg/s/g} \left( \frac{t}{1 \text{ day}} \right)^{-1} \left( \frac{X_{A \geq 250}}{2 \cdot 10^{-2}} \right). \quad (5)$$

where  $X_{A \geq 210}$  ( $X_{A \geq 250}$ ) is the total mass fraction of nuclei with  $210 \leq A \leq 280$  ( $250 \leq A \leq 280$ ). Note that the numerical coefficients in Eqs. (2) and (3) are valid as long as material has the solar-like  $r$ -process pattern containing the second ( $A \sim 130$ ) and third ( $A \sim 195$ )  $r$ -process peaks.

Although the form of  $\epsilon_{\gamma}(t)$  should be computed with a radiative transfer simulation, here we give rough estimates. The optical depth of homologously expanding ejecta is given by

$$\tau_{\gamma}(t) = \left( \frac{t_{\text{tr},\gamma}}{t} \right)^2, \quad (6)$$

where  $t_{\text{tr},\gamma} \approx (\kappa_{\gamma} M_{\text{ej}} / 4\pi v^2)^{1/2} \approx 0.4 \text{ day} (\kappa_{\gamma} / 0.05 \text{ cm}^2/\text{g})^{1/2} (M_{\text{ej}} / 0.01 M_{\odot})^{1/2} (v / 0.3c)^{-1}$  is the time that the ejecta become transparent to  $\gamma$ -rays.

Here we assume that the dominant interaction process of  $\gamma$ -rays with matter is Compton scattering.

At the diffuse-out timescale of thermal photons (optical to infrared: IR)  $t_{\text{diff},o}$  when the optical depth to thermal photons satisfies  $\tau_{\text{opt}} = c/v$ , a significant amount of the deposited energy starts to escape as thermal photons. We rewrite Eq. (6) in terms of  $t_{\text{diff},o}$ :

$$\tau_{\gamma}(t) \approx \frac{\kappa_{\gamma} c}{\kappa_o v} \left( \frac{t_{\text{diff},o}}{t} \right)^2, \quad (7)$$

$$\approx 0.02 \left( \frac{t_{\text{diff},o}}{t} \right)^2 \left( \frac{\kappa_{\gamma}}{0.05 \text{ cm}^2/\text{g}} \right) \times \left( \frac{\kappa_o}{10 \text{ cm}^2/\text{g}} \right)^{-1} \left( \frac{v}{0.3c} \right)^{-1}, \quad (8)$$

where  $\kappa_o$  is the opacity of  $r$ -process elements to photons in the optical bands. It is dominated by bound-bound transitions of lanthanides (Kasen et al. 2013; Tanaka & Hotokezaka 2013). For the dynamical ejecta, on the timescale of  $t_{\text{diff},o}$ , the optical depth to  $\gamma$ -rays is much smaller than unity, thereby only a small fraction of the  $\gamma$ -rays' energy is deposited in the ejecta on the peak timescale of macronovae.

For the slowly expanding wind ejecta, in particular lanthanide free cases, the  $\gamma$ -ray heating efficiency is significantly different. The opacity to thermal photons and expansion velocity of the wind ejecta are  $\kappa_o \sim 1 \text{ cm}^2/\text{g}$  and  $v \sim 0.05c$  (see

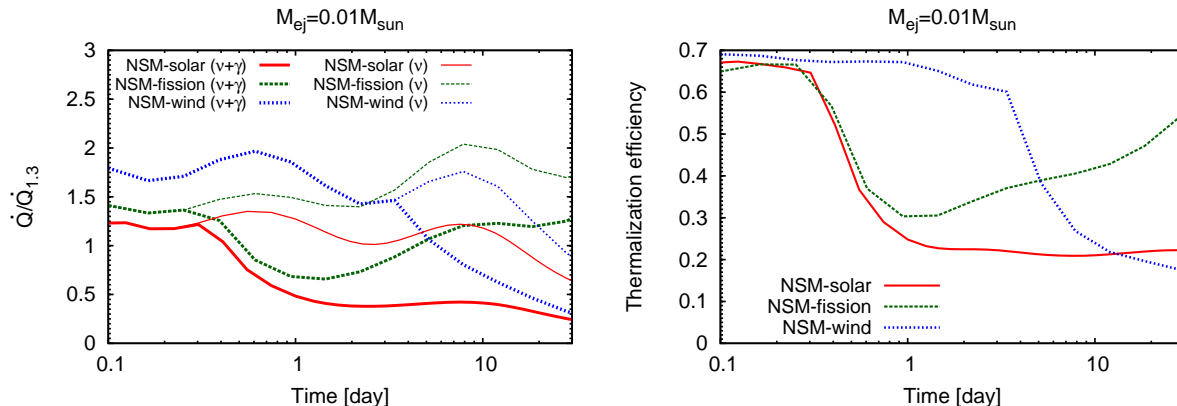


**Figure 3.** Heating rate normalized by  $\dot{Q}_{1.3}(t) = 10^{10} t_{\text{day}}^{-1.3}$  erg/s/g (left), where  $t_{\text{day}}$  is time in unit of day, and thermalization efficiency (right) for each model: NSM-solar (red solid), NSM-fission (green dashed), and NSM-wind (blue dotted). The thick (thin) lines in the left panel show the heating rate taking the neutrino and gamma-ray escape (only the neutrino escape) into account. For the gamma-ray escape, an ejecta mass of  $0.01M_{\odot}$  is assumed as an example.

e.g., Tanaka & Hotokezaka 2013 for the opacity of the wind case). The estimated optical depth to  $\gamma$ -rays is  $\tau_{\gamma} \sim 3$  on the timescale of  $t_{\text{diff},o}$ . Therefore, in the case of the lanthanide free wind ejecta,  $\gamma$ -rays are weakly coupled with the ejected material and heat up the ejecta until a few times  $t_{\text{diff},o}$ . This situation is somewhat similar to those of supernovae, in which  $\gamma$ -rays released from the radioactive decay of  $^{56}\text{Ni}$  and  $^{56}\text{Co}$  efficiently heat up the ejecta on the peak timescale of supernovae (Lucy 2005).

Here we approximately evaluate  $\epsilon_{\gamma}(t)$  as the followings. In optically thick regimes  $\tau_{\gamma} \gg 1$ , almost all the  $\gamma$  rays' energy is deposited in the ejecta. On the contrary, in optically thin regimes  $\tau_{\gamma} < 1$ , only a fraction  $\tau$  of the photons are scattered and for each scattered photon roughly half of  $\gamma$  ray's energy is transferred to an electron via a single scattering process at energies of  $\sim 1$  MeV.  $\epsilon_{\gamma}$  is approximately given by

$$\epsilon_{\gamma}(t) \approx \begin{cases} 1 - \left(\frac{1}{2}\right)^N & (\tau_{\gamma} \geq 1), \\ \frac{1}{2}N & (\tau_{\gamma} < 1), \end{cases} \quad (9)$$

where  $N = \max(\tau_{\gamma}, \tau_{\gamma}^2)$  is the number of the scatterings that a photon undergoes before escaping. Figure 3 shows the heating rate (left) and the thermalization efficiency (right). Here the heating rate is normalized by a simple power law heating  $\dot{Q}_{1.3}(t) = 10^{10} t_{\text{day}}^{-1.3}$  erg/s/g (Korobkin et al. 2012), where  $t_{\text{day}}$  is time in unit of day. The thick (thin) lines in the left panel show the heating rate taking the neutrino and gamma-ray escape (only the neutrino escape) into account. To calculate  $\epsilon_{\gamma}(t)$ , an ejecta mass of  $0.01M_{\odot}$  is assumed. The velocities of the ejecta is set to be  $0.3c$  for NSM-solar and NSM-fission and  $0.05c$  for NSM-wind. For NSM-solar and NSM-fission, at 0.5 days,  $\gamma$ -rays start to escape from the ejecta so that the thermalization efficiency drops from 0.7 to 0.2 – 0.3. The heating rate and thermalization efficiency of NSM-wind are larger than the other cases since  $\gamma$ -rays are well scattered. For NSM-fission, the thermalization efficiency turns to increase due to the spontaneous fission of transuranic nuclei and it reaches  $\approx 0.5$  around 10 days.

#### 4 IMPLICATION TO THE POSSIBLE MACRONOVA EVENTS

Assuming a constant thermalization efficiency of 0.5, the minimal masses of ejected  $r$ -process material are estimated as  $\approx 0.02M_{\odot}$  for GRB 130603B (Hotokezaka et al. 2013a; Piran et al. 2014) and  $\approx 0.1M_{\odot}$  for GRB 060614 (Yang et al. 2015), where the large lanthanide opacity is taken into account (Kasen et al. 2013; Barnes & Kasen 2013; Tanaka & Hotokezaka 2013). These estimates change once we use the thermalization efficiencies that we obtained here. The IR detections were done at 7 days for GRB 130603B and at 12 days for GRB 060614 after the bursts in the GRBs' rest frames. For NSM-solar, the heat is provided only through electrons so that the thermalization efficiency at this timescale is  $\approx 0.2$  (see Fig. 3). The minimal required masses are larger than what previously estimated by a factor of  $\approx 2.5$ . As a result, the estimated masses are  $0.05M_{\odot}$  and  $0.25M_{\odot}$  respectively. The former may be explained in the context of the black-hole neutron star merger ejecta. However, the latter is too large for the compact binary merger ejecta. Therefore, in addition to  $\beta$ -decay, other sources of energy injection may be required to explain this event as a compact binary merger.

The spontaneous fission of transuranic nuclei can increase the heating rates at later times as discussed earlier. For NSM-fission, for which the mass fraction of transuranic nuclei is  $\approx 0.02$ , the heating rate at 10 days is larger than that of NSM-solar by a factor of  $\approx 3$  (see the left panel of Fig. 3). Based on NSM-fission, therefore, the minimal required masses are smaller than the ones of NSM-solar by a factor of 3 and similar to what estimated in the previous works (Hotokezaka et al. 2013a; Piran et al. 2014; Yang et al. 2015). However, there are large uncertainties in the fission and  $\beta$ -decay lifetimes of transuranic nuclei (Wanajo et al. 2014) as well as the abundance distribution (Eichler et al. 2015). Thus these estimates are uncertain.

It is also worthy to mention that there are alternative scenarios to inject additional energy from the central

engine activity, e.g., X-ray irradiation (Kisaka et al. 2015) and magnetar outflows (Fan et al. 2013; Metzger & Piro 2014; Gao et al. 2015). Because the central engine models predict observable signatures in the multi-wavelength, to identify the dominant energy source of macronovae, X-ray observations on the macronova peak timescale and late-time radio observations (months to years) are important. In fact, the late time radio upper limits have already constrained the magnetar engine model for GRB 130603B and 060614 (Fong et al. 2014; Horesh et al. 2015)

## 5 DETECTABILITY OF $\gamma$ -RAYS OF $r$ -PROCESS NUCLIDES

Given that the  $\gamma$ -rays escape from the ejecta we turn now to compute the light curves of  $\gamma$ -rays escaping directly from radioactive decay, i.e.,  $\gamma$ -rays produced outside their photosphere (Clayton et al. 1969). For these  $\gamma$ -rays, the observed spectrum preserves the original shape (see Fig. 2). To identify the radius of the photosphere of each energy band, we take into account three processes of  $\gamma$ -rays with matter: (i) the photoelectric absorption ( $E_\gamma \lesssim 300$  keV), (ii) Compton scattering ( $E_\gamma \sim 1$  MeV), and (iii) the pair production ( $E_\gamma \gtrsim 5$  MeV). The photoelectric absorption dominates in the low energy range and depends on the composition of material. The mass absorption coefficient of the photoelectric absorption for  $r$ -process material with the solar abundance pattern ( $40 \leq Z \leq 92$ ) is shown in Fig. 4. At high energies  $E_\gamma \gtrsim 100$  keV, the mass absorption coefficient  $\kappa_{\text{ph}}$  is approximately described by  $\kappa_{\text{ph}} \approx 2.5 \text{ cm}^2/\text{g} (E_\gamma/100 \text{ keV})^{-2.7}$ . At low energies  $E_\gamma \lesssim 100$  keV,  $\kappa_{\text{ph}} \approx 2.5 \text{ cm}^2/\text{g} (E_\gamma/100 \text{ keV})^{-1.8}$  (see NIST database<sup>3</sup> for the mass absorption coefficient for each element). Here the density structure of ejecta is assumed as  $\rho \propto r^{-3}$  and the maximum velocity is set to be twice of the average velocity.

Figure 5 shows the  $\gamma$ -ray fluxes for an observer at a distance of 3 Mpc in the four different energy bands,  $10 \text{ keV} \leq E_\gamma < 30 \text{ keV}$  (top left),  $30 \text{ keV} \leq E_\gamma < 100 \text{ keV}$  (top right),  $100 \text{ keV} \leq E_\gamma < 300 \text{ keV}$  (bottom left), and  $300 \text{ keV} \leq E_\gamma < 1 \text{ MeV}$  (bottom right). Here we show the four different ejecta models:  $(M_{\text{ej}}, v) = (0.01 M_\odot, 0.3c)$ ,  $(0.01 M_\odot, 0.05c)$ ,  $(0.1 M_\odot, 0.3c)$ , and  $(0.1 M_\odot, 0.05c)$ . Because the photospheric radius depends strongly on the  $\gamma$ -ray's energy, the peak timescales of  $\gamma$ -ray fluxes are different for different energy bands. For  $10 \text{ keV} \leq E_\gamma < 30 \text{ keV}$ , the peak time is as late as 30 days to 100 days. On the contrary, for  $300 \text{ keV} \leq E_\gamma < 1 \text{ MeV}$ , the  $\gamma$ -ray flux peaks around 1–10 days. Because more energy is released in  $\gamma$ -rays at higher energies and they escape from the ejecta at earlier times than at lower energies, the detections may be easier at the higher energy bands.

Here we compare the expected fluxes of events with the sensitivity of current-and-future missions in the 30 keV–1 MeV range, i.e., *ASTRO-H* HXI (pre-launch) and *NuSTAR* for 30–100 keV (Takahashi et al. 2012; Harrison et al. 2013), *ASTRO-H* SGD (pre-launch) for 100 keV–1 MeV (Takahashi et al. 2012), and *CAST* for

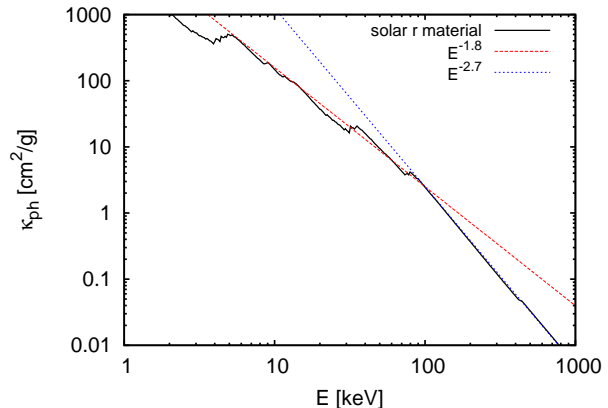


**Figure 4.** Mass absorption coefficient of photoelectric absorption. Here we assume that the material is composed of  $r$ -process elements with  $40 \leq Z \leq 92$  and the abundance pattern is the solar pattern of stable and long-lived  $r$ -process nuclei.

300 keV–1 MeV (Nakazawa et al. 2014). The resultant sensitivities are shown with the dotted lines Fig. 5 assuming each exposure at 100 ks, since the expected fluxes show the variabilities on timescales of  $\sim 100$  ks.  $\gamma$ -rays are detectable at 300 keV to 1 MeV with *ASTRO-H*SGD and *CAST* for an event at a distance of 3 Mpc with an ejecta mass of  $0.1 M_\odot$ . For *CAST*, it is detectable even for an event at 10 Mpc with  $0.1 M_\odot$  and at 3 Mpc with  $0.01 M_\odot$ . However, the rate of such nearby events ( $\lesssim 3$  Mpc) is small, e.g., an optimistic estimate gives  $\sim 10^{-3} \text{ yr}^{-1}$  (Abadie et al. 2010). Therefore, new detectors, more sensitive by at least a factor of ten, are needed for a realistic detection rate of these signals.

## 6 CONCLUSION

We studied the radioactive decay products of heavy  $r$ -process nuclei in neutron star merger ejecta on timescales from hours to a month. We found that 30–40% of the energy is released in neutrinos and lost. Electrons carry 10–20% of the energy. These always deposit their energy in the ejecta and hence this provides a lower limit on the energy fraction deposited in the ejecta. In the case that transuranic nuclei with mass numbers of  $A > 238$  exist, spontaneous fission products can carry a significant fraction of the energy after a few days. At a week after the merger this fraction of the total energy can be 20% when the total mass fraction of nuclei with  $238 < A \leq 280$  is 2%. It should be noted, however, the contribution of spontaneous fission is highly dependent on several experimentally unknown fission and  $\beta$ -decay lifetimes (Wanajo et al. 2014) as well as the abundance distribution (Eichler et al. 2015) in this range.

$\gamma$ -rays carry 20–50% of the energy. The number of  $\gamma$ -ray photons is roughly constant per unit energy interval from a few dozen keV to 1 MeV. Thus the energy is dominated by 1 MeV photons. The heating efficiency of  $\gamma$ -rays depends on the ejecta properties. For the rapidly expanding ejecta (e.g. dynamical ejecta), only a small fraction (a few percent) of the  $\gamma$ -rays' energy is deposited at a few days, that is during the peak of the optical–IR emission. On the contrary, a large fraction of the energy may be deposited in a slowly expanding lanthanide-

<sup>3</sup> <http://www.nist.gov/pml/data/ffast/index.cfm>

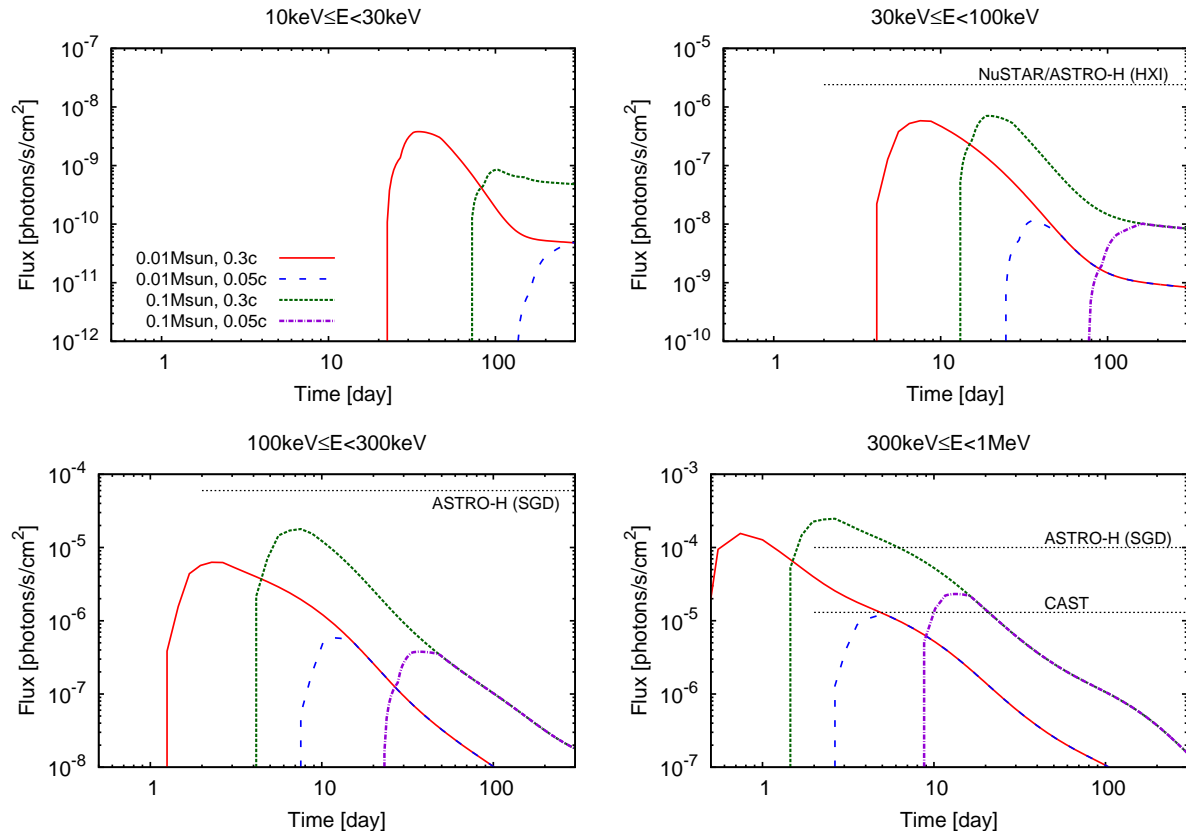


**Figure 5.** Light curves of nuclear  $\gamma$ -rays for NSM-solar in the ranges of  $10 \text{ keV} \leq E_\gamma < 30 \text{ keV}$  (top left),  $30 \text{ keV} \leq E_\gamma < 100 \text{ keV}$  (top right),  $100 \text{ keV} \leq E_\gamma < 300 \text{ keV}$  (bottom left), and  $300 \text{ keV} \leq E_\gamma < 1 \text{ MeV}$  (bottom right) at a distance of 3 Mpc. Here we show the four different ejecta models:  $(M_{\text{ej}}, v) = (0.01 M_\odot, 0.3c)$ ,  $(0.01 M_\odot, 0.05c)$ ,  $(0.1 M_\odot, 0.3c)$ , and  $(0.1 M_\odot, 0.05c)$ . Also shown are the sensitivity with exposure at 100 ks of current and future X-ray missions: *NuSTAR* (Harrison et al. 2013), *ASTRO-H* (Takahashi et al. 2012), and *CAST* (Nakazawa et al. 2014).

free ejecta at the corresponding time of the peak. Such ejecta could be the cases for the late-time wind from NSM remnants (Metzger & Fernández 2014; Perego et al. 2014; Sekiguchi et al. 2015; Foucart et al. 2015) or from black-hole accretion torii (Wanaajo & Janka 2012; Just et al. 2015; Fernández et al. 2015; Kasen et al. 2015)

Full radiation transfer simulations are needed in order to obtain the time evolution of the  $\gamma$ -ray energy deposition fraction. But even without these detailed calculations it is evident that radiation losses of the  $\gamma$ -ray emission will reduce the strength of the optical/IR luminosity of the dynamical ejecta, namely the expected macronova signature to about two thirds to a half from its original estimates, assuming that this energy is absorbed by the ejecta and re-radiated at low energies. For observed signals with a given luminosity (e.g. the macronova candidates 130603B Tanvir et al. 2013; Berger et al. 2013 and 060614 Yang et al. 2015), this means that the implied mass should be larger than what was earlier estimated by a factor of two to three. If a sufficient amount of transuranic nuclei are synthesized, the spontaneous fission products contribute the heating rate on the macronova timescales and the estimated mass can be similar to the previous estimates. Alternatively, energy injection from the central engine activity can also contribute to power the op-

tical/IR transients (Fan et al. 2013; Metzger & Piro 2014; Kisaka et al. 2015; Gao et al. 2015).

The peak timescale of the flux of the of the escaping  $\gamma$ -rays depends significantly on the energy band. For  $\gamma$ -rays at higher energies of 300 keV to 1 MeV, the peak timescale is days to a few dozen days. Due to the photoelectric absorption, the peak time for lower energies of 10 keV to 30 keV, is a month to a year. The corresponding flux of  $\gamma$ -rays at energies of 300 keV to 1 MeV from a merger event with an ejecta mass of  $0.1 M_\odot$  are detectable with *ASTRO-H* SGD and *CAST* if it happens at 3 Mpc and at 10 Mpc, respectively. Direct measurements of these  $\gamma$ -rays may provide ultimate proof of the macronova mechanisms and the sites of  $r$ -process nucleosynthesis. However, such a nearby event is too rare to be detected with current detectors. This detection with a realistic rate will have to wait for a more sensitive generation that may be launched in the future.

## ACKNOWLEDGMENTS

We thank Ben Margalit, Satoshi Chiba, and Re'em Sari for discussions. This research was supported by the I-CORE Program of the Planning and Budgeting Committee and The Israel Science Foundation (grant No 1829/12), the RIKEN iTHES Project, and Grants-in-Aid for Scientific Re-

search of JSPS (26400232, 26400237, 15H02075) and MEXT (15H00788, 15H00773, 15K05107).

## REFERENCES

- Abadie J., Abbott B. P., Abbott R., Abernathy M., Accadia T., Acernese F., Adams C., Adhikari R., Ajith P., Allen B., et al. 2010, *Classical and Quantum Gravity*, 27, 173001
- Argast D., Samland M., Thielemann F.-K., Qian Y.-Z., 2004, *A&A*, 416, 997
- Arnould M., Goriely S., Takahashi K., 2007, *Phys. Rep.*, 450, 97
- Barbuy B., Spite M., Hill V., Primas F., Plez B., Cayrel R., Spite F., Wanajo S., Siqueira Mello C., Andersen J., Nordström B., Beers T. C., Bonifacio P., François P., Molero P., 2011, *A&A*, 534, A60
- Barnes J., Kasen D., 2013, *ApJ*, 775, 18
- Bauswein A., Goriely S., Janka H.-T., 2013, *ApJ*, 773, 78
- Berger E., Fong W., Chornock R., 2013, *ApJL*, 774, L23
- Berger E., 2014, *ARA&A*, 52, 43
- Brennecke G. A., Weyer S., Wadhwa M., Janney P. E., Zipfel J., Anbar A. D., 2010, *Science*, 327, 449
- Churazov E., Sunyaev R., Isern J., Knödlseher J., Jean P., Lebrun F., Chugai N., Grebenev S., Bravo E., Sazonov S., Renaud M., 2014, *Nature*, 512, 406
- Clayton D. D., Colgate S. A., Fishman G. J., 1969, *ApJ*, 155, 75
- Cowan J. J., Pfeiffer B., Kratz K.-L., Thielemann F.-K., Sneden C., Burles S., Tytler D., Beers T. C., 1999, *ApJ*, 521, 194
- Cowan J. J., Thielemann F.-K., Truran J. W., 1991, *Phys. Rep.*, 208, 267
- Diehl R., Siebert T., Hillebrandt W., Grebenev S. A., Greiner J., Krause M., Kromer M., Maeda K., Röpke F., Taubenberger S., 2014, *Science*, 345, 1162
- East W. E., Paschalidis V., Pretorius F., Shapiro S. L., 2015, *ArXiv e-prints*
- Eichler D., Livio M., Piran T., Schramm D. N., 1989, *Nature*, 340, 126
- Eichler M., Arcones A., Kelic A., Korobkin O., Langanke K., Marketin T., Martínez-Pinedo G., Panov I., Rauscher T., Rosswog S., Winteler C., Zinner N. T., Thielemann F.-K., 2015, *ApJ*, 808, 30
- Fan Y.-Z., Yu Y.-W., Xu D., Jin Z.-P., Wu X.-F., Wei D.-M., Zhang B., 2013, *ApJL*, 779, L25
- Fernández R., Kasen D., Metzger B. D., Quataert E., 2015, *MNRAS*, 446, 750
- Fernández R., Metzger B. D., 2013, *MNRAS*
- Fong W., Berger E., Metzger B. D., Margutti R., Chornock R., Migliori G., Foley R. J., Zauderer B. A., Lunnan R., Laskar T., Desch S. J., Meech K. J., Sonnett S., Dickey C., Hedlund A., Harding P., 2014, *ApJ*, 780, 118
- Foucart F., Deaton M. B., Duez M. D., Kidder L. E., MacDonald I., Ott C. D., Pfeiffer H. P., Scheel M. A., Szilagyi B., Teukolsky S. A., 2013, *Phys. Rev. D.*, 87, 084006
- Foucart F., Haas R., Duez M. D., O'Connor E., Ott C. D., Roberts L., Kidder L. E., Lippuner J., Pfeiffer H. P., Scheel M. A., 2015, *ArXiv e-prints*
- Freiburghaus C., Rosswog S., Thielemann F.-K., 1999, *ApJL*, 525, L121
- Gao H., Ding X., Wu X.-F., Dai Z.-G., Zhang B., 2015, *ApJ*, 807, 163
- Goriely S., Bauswein A., Just O., Pllumbi E., Janka H.-T., 2015, *MNRAS*, 452, 3894
- Goriely S., Sida J.-L., Lemaître J.-F., Panebianco S., Dubray N., Hilaire S., Bauswein A., Janka H.-T., 2013, *Physical Review Letters*, 111, 242502
- Grossman D., Korobkin O., Rosswog S., Piran T., 2014, *MNRAS*, 439, 757
- Harrison F. A., et al. 2013, *ApJ*, 770, 103
- Hirai Y., Ishimaru Y., Saitoh T. R., Fujii M. S., Hidaka J., Kajino T., 2015, *ArXiv e-prints*
- Horesh, et al., 2015, in preparation
- Hotkezaka K., Kiuchi K., Kyutoku K., Okawa H., Sekiguchi Y.-i., Shibata M., Taniguchi K., 2013, *Phys. Rev. D.*, 87, 024001
- Hotkezaka K., Kyutoku K., Tanaka M., Kiuchi K., Sekiguchi Y., Shibata M., Wanajo S., 2013a, *ApJL*, 778, L16
- Hotkezaka K., Piran T., Paul M., 2015, *ArXiv e-prints*
- Ishimaru Y., Wanajo S., Prantzos N., 2015, *ApJL*, 804, L35
- Just O., Bauswein A., Pulpillo R. A., Goriely S., Janka H.-T., 2015, *MNRAS*, 448, 541
- Kalogera V., Kim C., Lorimer D. R., Burgay M., D'Amico N., Possenti A., Manchester R. N., Lyne A. G., Joshi B. C., McLaughlin M. A., Kramer M., Sarkissian J. M., Camilo F., 2004, *ApJL*, 601, L179
- Kasen D., Badnell N. R., Barnes J., 2013, *ApJ*, 774, 25
- Kasen D., Fernández R., Metzger B. D., 2015, *MNRAS*, 450, 1777
- Kawaguchi K., Kyutoku K., Nakano H., Okawa H., Shibata M., Taniguchi K., 2015, *Phys. Rev. D.*, 92, 024014
- Kim C., Perera B. B. P., McLaughlin M. A., 2015, *MNRAS*, 448, 928
- Kisaka S., Ioka K., Nakar E., 2015, *ArXiv e-prints*
- Kiuchi K., Sekiguchi Y., Kyutoku K., Shibata M., Taniguchi K., Wada T., 2015, *Phys. Rev. D.*, 92, 064034
- Korobkin O., Rosswog S., Arcones A., Winteler C., 2012, *MNRAS*, 426, 1940
- Kyutoku K., Ioka K., Okawa H., Shibata M., Taniguchi K., 2015, *ArXiv e-prints*
- Lattimer J. M., Schramm D. N., 1976, *ApJ*, 210, 549
- Li L.-X., Paczyński B., 1998, *ApJL*, 507, L59
- Lippuner J., Roberts L. F., 2015, *ArXiv e-prints*
- Lucy L. B., 2005, *A&A*, 429, 19
- Matz S. M., Share G. H., Leising M. D., Chupp E. L., Vestrand W. T., 1988, *Nature*, 331, 416
- Metzger B. D., Fernández R., 2014, *MNRAS*, 441, 3444
- Metzger B. D., Martínez-Pinedo G., Darbha S., Quataert E., Arcones A., Kasen D., Thomas R., Nugent P., Panov I. V., Zinner N. T., 2010, *MNRAS*, 406, 2650
- Metzger B. D., Piro A. L., 2014, *MNRAS*, 439, 3916
- Nakar E., 2007, *Phys. Rep.*, 442, 166
- Nakazawa K., et al. 2014, in *Society of Photo-Optical Instrumentation Engineers (SPIE) Conference Series Vol. 9144 of Society of Photo-Optical Instrumentation Engineers (SPIE) Conference Series, Sub-MeV all sky survey with a compact Si/CdTe Compton telescope*.p. 0
- Perego A., Rosswog S., Cabezón R. M., Korobkin O., Käppeli R., Arcones A., Liebendörfer M., 2014, *MNRAS*, 443, 3134
- Piran T., Korobkin O., Rosswog S., 2014, *ArXiv e-prints*

- Qian Y.-Z., Wasserburg G. J., 2007, *Phys. Rep.*, 442, 237
- Roberts L. F., Kasen D., Lee W. H., Ramirez-Ruiz E., 2011, *ApJL*, 736, L21
- Roederer I. U., Schatz H., Lawler J. E., Beers T. C., Cowan J. J., Frebel A., Ivans I. I., Sneden C., Sobeck J. S., 2014, *ApJ*, 791, 32
- Rosswog S., 2013, *Royal Society of London Philosophical Transactions Series A*, 371, 20272
- Sekiguchi Y., Kiuchi K., Kyutoku K., Shibata M., 2015, *Phys. Rev. D.*, 91, 064059
- Shen S., Cooke R. J., Ramirez-Ruiz E., Madau P., Mayer L., Guedes J., 2015, *ApJ*, 807, 115
- Shibata M., Suwa Y., Kiuchi K., Ioka K., 2011, *ApJL*, 734, L36
- Siegel D. M., Ciolfi R., Rezzolla L., 2014, *ApJL*, 785, L6
- Siqueira Mello C., Hill V., Barbay B., Spite M., Spite F., Beers T. C., Caffau E., Bonifacio P., Cayrel R., François P., Schatz H., Wanajo S., 2014, *A&A*, 565, A93
- Sneden C., Cowan J. J., Gallino R., 2008, *ARA&A*, 46, 241
- Symbalisty E., Schramm D. N., 1982, *ApJL*, 22, 143
- Takahashi T., et al. 2012, in *Society of Photo-Optical Instrumentation Engineers (SPIE) Conference Series Vol. 8443 of Society of Photo-Optical Instrumentation Engineers (SPIE) Conference Series, The ASTRO-H X-ray Observatory*. p. 1
- Tanaka M., Hotokezaka K., 2013, *ApJ*, 775, 113
- Tanaka M., Hotokezaka K., Kyutoku K., Wanajo S., Kiuchi K., Sekiguchi Y., Shibata M., 2014, *ApJ*, 780, 31
- Tanvir N. R., Levan A. J., Fruchter A. S., Hjorth J., Hounsell R. A., Wiersema K., Tunncliffe R. L., 2013, *Nature*, 500, 547
- Teegarden B. J., Barthelmy S. D., Gehrels N., Tueller J., Leventhal M., 1989, *Nature*, 339, 122
- Terada Y., Maeda K., Fukazawa Y., et al., 2015, *ApJ*, submitted
- Tsujimoto T., Shigeyama T., 2014, *A&A*, 565, L5
- Turner G., Busfield A., Crowther S. A., Harrison M., Mojzsis S. J., Gilmour J., 2007, *Earth and Planetary Science Letters*, 261, 491
- Turner G., Harrison T. M., Holland G., Mojzsis S. J., Gilmour J., 2004, *Science*, 306, 89
- van de Voort F., Quataert E., Hopkins P. F., Kereš D., Faucher-Giguère C.-A., 2015, *MNRAS*, 447, 140
- Wallner A., Faestermann T., Feige J., Feldstein C., Knie K., Korschinek G., Kutschera W., Ofan A., Paul M., Quinto F., Rugel G., Steier P., 2015, *Nature Communications*, 6, 5956
- Wanajo S., Ishimaru Y., 2006, *Nuclear Physics A*, 777, 676
- Wanajo S., Janka H.-T., 2012, *ApJ*, 746, 180
- Wanajo S., Sekiguchi Y., Nishimura N., Kiuchi K., Kyutoku K., Shibata M., 2014, *ApJL*, 789, L39
- Wanderman D., Piran T., 2015, *MNRAS*, 448, 3026
- Wehmeyer B., Pignatari M., Thielemann F.-K., 2015, *MNRAS*, 452, 1970
- Yang B., Jin Z.-P., Li X., Covino S., Zheng X.-Z., Hotokezaka K., Fan Y.-Z., Piran T., Wei D.-M., 2015, *Nature Communications*, 6, 7323